

RESEARCH ARTICLE

10.1002/2016WR019341

Impact of mountain permafrost on flow path and runoff response in a high alpine catchment

M. Rogger¹ , G. B. Chirico² , H. Hausmann^{3,4}, K. Krainer⁵, E. Brückl⁴, P. Stadler⁶, and G. Blöschl¹

Key Points:

- The occurrence of Alpine permafrost is related to different types of unconsolidated sediment
- Four concepts of dominant flow paths in hillslopes are proposed for different subsurface and permafrost characteristics
- Disappearance of Alpine permafrost will decrease flood peaks and increase runoff during recession

Correspondence to:

M. Rogger,
rogger@hydro.tuwien.ac.at

Citation:

Rogger, M., G. B. Chirico, H. Hausmann, K. Krainer, E. Brückl, P. Stadler, and G. Blöschl (2017), Impact of mountain permafrost on flow path and runoff response in a high alpine catchment, *Water Resour. Res.*, 53, 1288–1308, doi:10.1002/2016WR019341.

Received 14 JUN 2016

Accepted 10 JAN 2017

Accepted article online 20 JAN 2017

Published online 3 FEB 2017

¹Institute for Hydraulic Engineering and Water Resources Management, Vienna University of Technology, Vienna, Austria, ²Dipartimento di Agraria, Università di Napoli Federico II, Naples, Italy, ³Zentralanstalt für Meteorologie und Geodynamik, Vienna, Austria, ⁴Institute of Geodesy and Geophysics, Vienna University of Technology, Vienna, Austria, ⁵Institute of Geology, University of Innsbruck, Innsbruck, Austria, ⁶Institute for Water Quality, Resources and Waste management, Vienna University of Technology, Vienna, Austria

Abstract Permafrost in high alpine catchments is expected to disappear in future warmer climates, but the hydrological impact of such changes is poorly understood. This paper investigates the flow paths and the hydrological response in a 5 km² high alpine catchment in the Ötztal Alps, Austria, and their changes resulting from a loss of permafrost. Spatial permafrost distribution, depth to the permafrost table, and depth to the bedrock were mapped by geophysical methods. Catchment runoff and meteorological variables were monitored from June 2008 to December 2011. These data were used along with field experience to infer conceptual schemes of the dominant flow paths in four types of hillslopes that differ in terms of their unconsolidated sediment characteristics and the presence of permafrost. The four types are: talus fans, rock glaciers, Little Ice Age (LIA) till, and pre-LIA till. Permafrost tends to occur in the first three types, but is absent from pre-LIA till. Based on these flow path concepts, runoff was simulated for present conditions and for future conditions when permafrost has completely disappeared. The simulations indicate that complete disappearance of permafrost will reduce flood peaks by up to 17% and increase runoff during recession by up to 19%. It is argued that change modeling needs to account for flow path types and their changes based on geophysical surveys and field investigations.

1. Introduction

Permafrost represents unconsolidated sediment or bedrock that remains frozen for at least two consecutive years. It is abundant in the high latitudes of the Northern Hemisphere [Gärtner-Roer *et al.*, 2010], but also occurs in high mountain areas where temperatures are low during all seasons [Cremonese *et al.*, 2011; Boeckli *et al.*, 2012]. Understanding the distribution of mountain permafrost and its influence on runoff behavior is important in the light of projected climate change [Haeberli *et al.*, 1993; Bary and Gan, 2011]. Alpine permafrost is likely to decrease during the next decades due to increasing temperatures [Harris *et al.*, 2003]. Some permafrost thawing has already been observed in the Northern Hemisphere [Nelson, 2003; Hinzman *et al.*, 2005; Zhang *et al.*, 2005; Anisimov and Reneva, 2006; Romanovsky *et al.*, 2010].

Because of their steep topography and past glacial processes, alpine catchments are often characterized by large amounts of sediment, such as talus slopes and various types of tills, which influence the runoff generation of the catchment by their storage behavior [Clow *et al.*, 2003; McClymont *et al.*, 2010; Liu *et al.*, 2004]. Most of the water from snowmelt and rain flows through the ground before it enters a stream [Campbell *et al.*, 1995; Sueker *et al.*, 2000; Liu *et al.*, 2004]. Permafrost in such settings may influence the storage capacity and subsurface flow paths and consequently the overall runoff response of a catchment [Koch *et al.*, 2013].

While the overall response of catchments to permafrost thawing is still poorly understood, a number of studies have examined specific aspects of mountain permafrost systems. A few studies have focused on identifying flow paths in different types of alpine sediments, such as moraines and rock glaciers. McClymont *et al.* [2011] identified three flow path types in a proglacial moraine in the Canadian Rockies based on geophysical measurements: shallow flow over margins of bedrock channels and buried ice; flow through the moraine over bedrock; and a possible flow path through a network of fractures in the bedrock. Langston *et al.* [2011] continued their research and suggested that the majority of the groundwater flows through a thin saturated layer at the moraine-bedrock interface or moraine-ice interface, while some water percolates

to deeper layers forming a deep groundwater table. *Krainer and Mostler* [2002] identified two storage reservoir types in rock glaciers in the Austrian Alps based on discharge and electrical conductivity measurements and dye tracer tests: a groundwater reservoir in a lower finer-grained layer that produces base flow; and a near-surface reservoir in a coarse-grained surface layer that produces near-surface runoff. They found subsurface flow velocities up to more than 300 m/h, indicating very large hydraulic conductivities of the coarse-grained upper layer. *Williams et al.* [2006] proposed a conceptual model of the flow paths in rock glaciers suggesting that the 0°C isotherm is near the surface at the beginning of the melting season and moves down during the summer, causing thawing of permafrost in the late summer and an increase in base flow. This conceptualization was confirmed by geophysical measurements of *Leopold et al.* [2011] on the same rock glacier. A better understanding of such flow paths in mountain permafrost catchments is an important prerequisite to improving hydrological models for such environments [*McClymont et al.*, 2011].

A number of studies have analyzed the influence of permafrost and permafrost degradation on runoff response. The presence of permafrost has been shown to reduce subsurface storage resulting in faster runoff response and larger event runoff coefficients [*McNamara et al.*, 1998]. The disappearance of permafrost due to permafrost thawing [*Lyon et al.*, 2009], on the other hand, has been shown to increase base flow and runoff during recession periods due to enhanced infiltration and deeper flow pathways [*Lyon and Destouni*, 2010; *Walvoord and Striegl*, 2007; *Evans et al.*, 2015], and to decrease seasonal runoff variability [*Frampton et al.*, 2011].

While these studies provide interesting insights into local permafrost environments and the associated runoff characteristics, very little is known about subsurface flow paths and permafrost distribution across an entire catchment and its influence on runoff response. By combining information from a detailed geological and geophysical field study in a high alpine catchment with distributed model simulations, this paper aims at: (a) understanding the permafrost distribution in a small alpine catchment; (b) understanding subsurface flow paths of different types of unconsolidated sediment with and without permafrost occurrence; and (c) analyzing the effect of permafrost disappearance on runoff dynamics. Section 2 of this paper presents the study area and data from the geological and geophysical field surveys and section 3 the geophysical analysis for mapping the permafrost distribution. On the basis of this information, section 4 proposes flow path concepts for different geologic formations which form the basis for the distributed hydrological model presented in section 5. The distributed model is used for assessing the catchment response under two scenarios: one in the current condition with permafrost and one assumes complete disappearance of the permafrost. The modeling results are presented and discussed in sections 5 and 6, respectively, and section 7 summarizes the conclusions of the study.

2. Study Area and Data

2.1. Study Area

The study area is the Krummgampen catchment in the Ötztal Alps (Tyrol, western Austria, 46°52'40N, 10°40'57E), a high alpine catchment (see photo Figure 1) with altitudes ranging from 2400 to 3350 m.a.s.l., and a mean annual air temperature of -0.5°C (recorded at a station near the catchment outlet). The catchment area is 5 km².

2.2. Geological Data and Sediment Properties

The geological characteristics of the catchment were mapped during a number of field surveys in the catchment. The geologic classes range from bedrock consisting of paragneiss, amphibolite and orthogneiss to different types of unconsolidated sediments such as talus slopes, intact and fossil rock glaciers, and two types of till deposits, pre-LIA (Little Ice Age) till and LIA till. The unconsolidated sediments cover more than 60% of the catchment area. During the field surveys, evidence of permafrost occurrence was found such as intact rock glaciers (locations indicated in Figure 2). Furthermore, patterned ground and solifluction lobes (Figure 2) indicate strong frost activity during a colder period in the past. Sediment samples from the top layer of the pre-LIA till, LIA till, and the steep fronts of the active rock glacier were collected during field surveys to perform grain size analysis.

2.3. Geophysical Data

In order to understand the permafrost distribution in the catchment, a number of seismic refraction and ground-penetrating radar measurements were performed. Both methods have been shown to be



Figure 1. Photo of the Krummgampen catchment in the Ötztal Alps, Austria (photo: Robert Illnar, view toward WSW).

particularly suited for detecting mountain permafrost [Musil *et al.*, 2002; Vonder Mühl *et al.*, 2002; Degenhardt and Giardino, 2003; Ikeda, 2006; Maurer and Hauck, 2007; Hilbich, 2010; Monnier *et al.*, 2011; Hausmann *et al.*, 2006, 2007, 2012; Hausmann and Behm, 2011; Krainer *et al.*, 2012a, 2012b, 2010a, 2010b].

A total of 32 seismic refraction profiles varying in lengths from 94 to 180 m were measured on talus, pre-LIA till, LIA till, and intact rock glacier areas (Figure 2). Three single recording units (REFTEK 130) with up to six channels were used to continuously record the waveforms from the seismic source. Two recording units—each connected to six omnidirectional geophones (Sensor SM-6/O-B, 14 Hz)—were deployed along the 32 profiles. Sufficient seismic energy was generated by hitting a plastic plate with a 5 kg hammer. The velocities of refracted waves estimated from the geophone response were then used to discriminate between various layer types and to identify ice and bedrock surfaces (see section 3). All seismic refraction measurements were conducted between mid July and mid October 2008 and 2009 at least 1 month after snowmelt.

Ground-penetrating radar (GPR) measurements were conducted using a GSSI SIR 3000 system over a total length of 4.2 km, covering pre-LIA till, LIA till, and intact rock glacier profiles (see Figure 2). A fixed antenna spacing of 4 m was used, with a spatial sampling interval of 1 m for rough terrain and a time-based collection mode with a marker interval of 5 m. The GPR measurements are complementary measurements to the seismic refraction data, to clearly identify the depth to the bedrock surface and thus the thickness of the sediment cover. Measurements were conducted on the rock glaciers in winter on a thick snow layer, when melt water was absent and on the till deposits in late summer to increase the penetration depth.

2.4. Ground Surface Temperature Data

Bottom temperatures of the winter snow cover (BTS) and the winter ground surface temperatures (wGST) have been used for a long time for permafrost mapping in mountain permafrost environments [e.g., King, 1984; Hoelzle, 1992, 1996; Tanarro *et al.*, 2001; Julian and Chueca, 2007]. In this study, winter ground surface temperatures (wGST) were measured by 27 HOBO Water Temp Pro v2 (U22-001) sensors continuously during the winters of 2007–2011 and used to estimate the Winter Equilibrium Temperature for the month where the snow cover is thick enough (>80 cm) to be insulating, following Haeberli [1973]. The

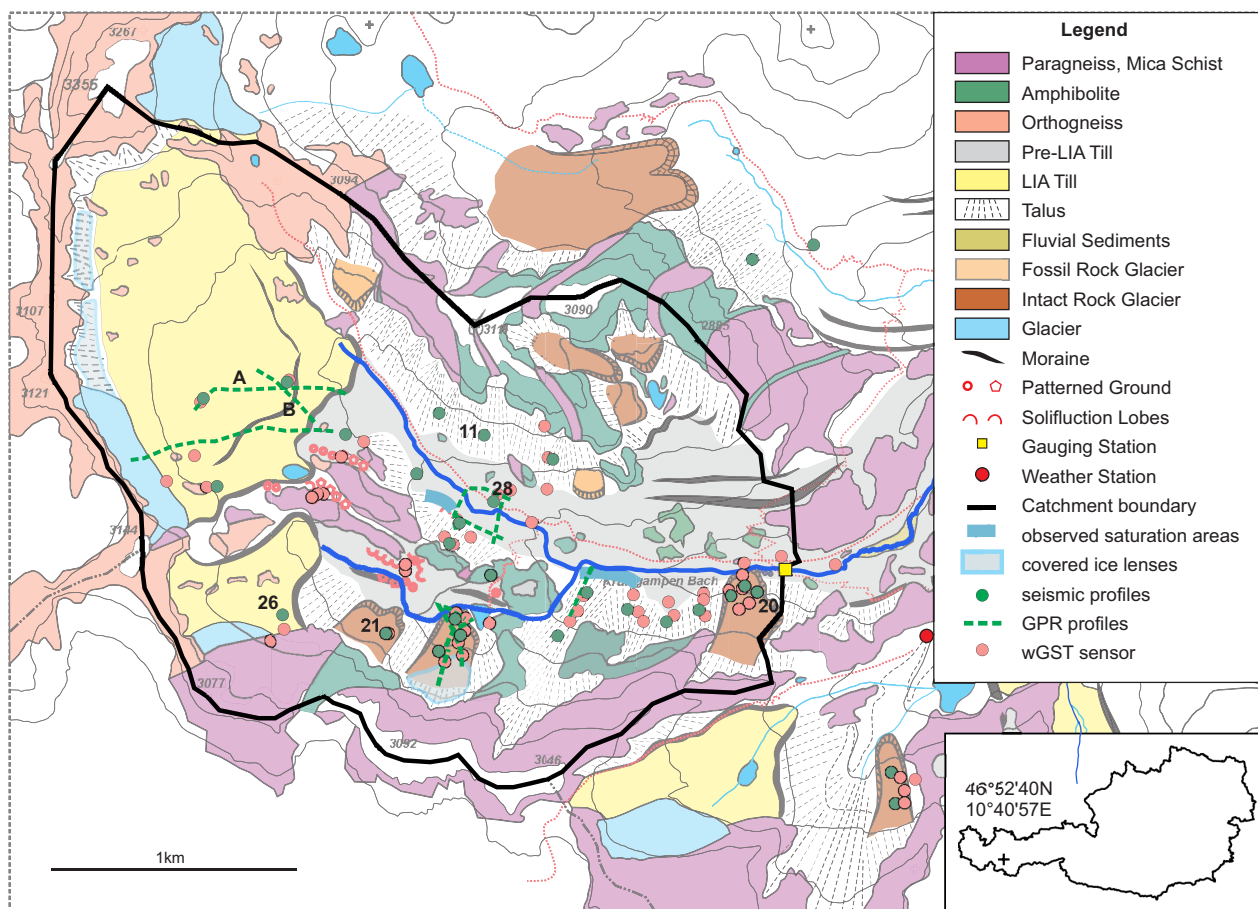


Figure 2. Geologic map of the Krummgampen catchment (Kauental, Western Ötztal Alps, Austria) indicating the locations of the geophysical field measurements; thick black line shows catchment boundary, inset map shows outline of Austria. The catchment area is 5 km².

sensors have an accuracy of $\pm 0.27^{\circ}\text{C}$, a resolution of 0.02°C , and a drift of 0.1°C per year. The temporal sampling rate was set to either 1 or 2 h and the data were corrected for drift. The locations of the sensors are indicated in Figure 2. Some of the sensors were relocated after each winter to measure different locations.

2.5. Hydrological Data and Runoff Regime

Stream water depth was recorded at the catchment outlet at an hourly interval by a pressure transducer. Stream discharge was calculated by a rating curve estimated from a number of salt dilution measurements at various water depths. For this study, data from June 2008 to December 2011 were used. Rainfall measured by a weighing type gauge and temperature data from a nearby weather station (Figure 2) were also available at hourly intervals.

Runoff at Krummgampen is dominated by snowmelt starting in late spring to early summer when daily mean temperatures rise above 0°C . The late summer runoff is due to rainfall events. Temperatures remain below 0°C from early autumn to late spring, causing the runoff to cease completely during the winter. A very small area (4%) of the catchment is covered by a glacier, but due to its small extent and northerly aspect, glacial melt is not deemed to affect runoff much. The mean observed runoff at the catchment outlet is 1500 mm/yr, the regional estimate of mean evaporation is about 200 mm/yr [BMLFUW, 2005], but mean observed precipitation at the weather station is only about 800 mm/yr. The geology does not indicate any subsurface leaking to neighboring catchments and annual precipitation from shielded rain gauges in the region at the same elevations are around 1500–1750 mm/a [Adler et al., 2015] which suggests a significant undercatch of the rain gauge during snowfall [see e.g., Sevruck, 1986; Nespor and Sevruck, 1999].

3. Geophysical Investigations

3.1. Methods

3.1.1. Data Processing

The raw GPR data were processed using the 2-D software ProMAX [Landmark Graphics Corporation, 1998]. The electromagnetic wave speeds were estimated by three different approaches: (a) by migration velocity analyses [Symes, 2008], (b) by measuring the curvature of reflection hyperbolae in the radargram sections, and (c) by common-midpoint measurements [Yilmaz, 1987]. Based on these analyses, mean wave speeds of 0.09–0.105 and 0.14 m/ns were estimated and used for the depth migration of the till areas and rock glaciers, respectively. Figures 3a and 3b show examples of the processed GPR data at LIA till profiles A and B.

For the processing of the seismic refraction data, two methods were applied:

The first is the conventional seismic refraction analysis methods (e.g., delay-time or generalized reciprocal method) [Gardner, 1939; Palmer, 1980; Sheehan et al., 2005], which requires assumptions about the number of layers and their compressional wave velocities, but is able to image sharp transitions between layers (i.e., accurate depth to the bedrock). In this study, a two-layered model was used to delineate the bedrock surface for permafrost-free profiles. For profiles where permafrost is present, a three-layered model was applied to resolve the bedrock surface and the depth to the permafrost table (e.g., on tills and rock glaciers). For this analysis, the ProMAX refraction statics calculation tool was used.

The second is the tomographic approach which requires specification of velocity gradients and is able to identify velocity variations resulting from heterogeneities in the subsurface. This was particularly important for some talus and rock glacier profiles, where permafrost occurred only in parts of the profile which cannot be resolved by the conventional method. However, the tomographic approach was applied to all profiles to double check whether any heterogeneities or lateral discontinuities were present. For this approach, the nonlinear 3-D travel time tomography [Hole, 1992] was used.

Figures 3c and 3d show examples of the processed seismic refraction data. The background colors show the compressional wave velocities from the tomographic approach, while the white labels and lines show the velocities from the conventional method (e.g., bedrock interface in Figure 3c and permafrost table in Figure 3d).

3.1.2. Permafrost Detection and Spatial Permafrost Distribution

Permafrost was identified by interpreting absolute values and changes with depth of compressional wave velocities and waveform stacks together with wGST.

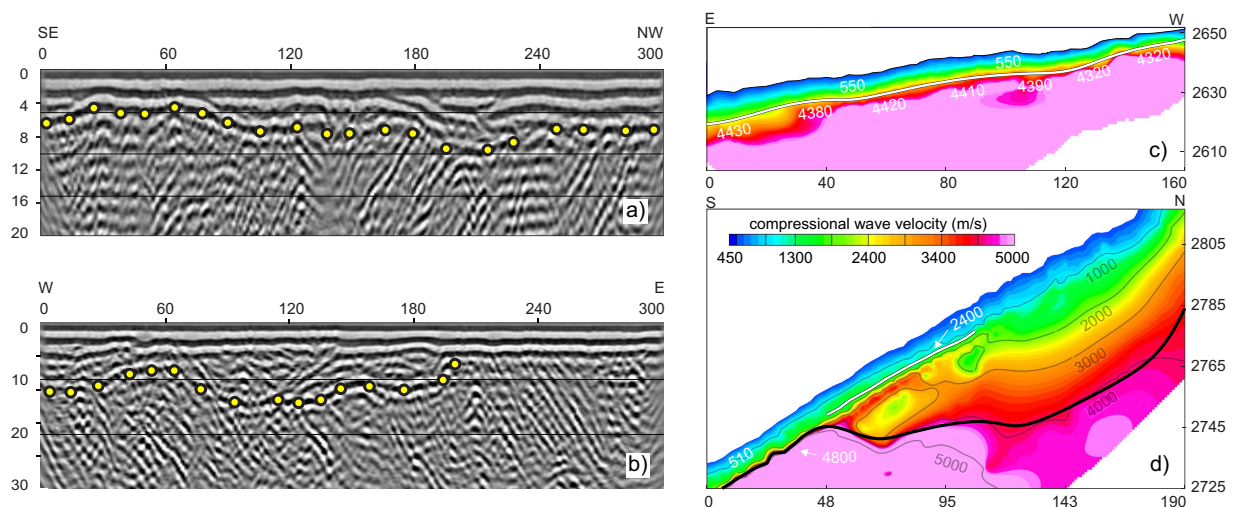


Figure 3. Examples of (a, b) processed GRP data and (c, d) seismic refraction data. GPR measurements at LIA till profiles (a) A and (b) B (see Figure 2 for location) with high-amplitude basal reflectors (yellow dots) that show the locations of the bedrock interface. Seismic refraction measurements at (c) pre-LIA till profile 28 and (d) talus slope 11 (see Figure 2 for location). Colors indicate compressional wave velocities from tomographic approach (velocities larger than 4000 m/s indicate bedrock, highlighted by black line); white numbers and white lines refer to velocities and interfaces from the conventional method.

In a first step, the presence of permafrost was detected for the locations of the seismic profiles. Compressional wave velocities increase significantly in frozen rocks and soils [Scott et al., 1990; Draebing and Krautblatter, 2012]. Typical values for unfrozen debris are 400–1000 m/s [e.g., Vonder Mühll et al., 2002; Hauck and Kneisel, 2008], for frozen talus slopes or degrading rock glaciers 1000–3000 m/s [Hauck and Kneisel, 2008], and for supersaturated ice in intact rock glaciers 3000–4000 m/s [Hauck and Kneisel, 2008; Hausmann et al., 2007, 2012]. The velocities for compact bedrock are even higher and range around 4400–5000 m/s [Vonder Mühll et al., 2002; Musil et al., 2002; Hausmann et al., 2007]. Winter ground surface temperatures (wGST) provide additional information on the presence of permafrost. wGST lower than -3°C indicate probable permafrost sites, values around -2°C indicate possible permafrost sites and values higher than -2°C indicate sites without permafrost [Haeberli, 1978]. By comparing compressional wave velocities and wGST by a manual cluster analysis, all profiles were classified into profiles with and profiles without permafrost.

In a second step, the presence of permafrost was regionalized from the seismic profile locations to the entire catchment. The regionalization used altitude and direct solar radiation which are good indicators of the presence of permafrost in mountain regions [Haeberli, 1975; Lugon and Delaloye, 2001; Julian and Chueca, 2007; Zhang et al., 2012]. The relationship of altitude and direct solar radiation was tested for the Krummgampen valley by using data from 145 rock glaciers from the Tyrolean rock glacier inventory [Krainer and Ribis, 2012] that are located in the surrounding valleys and have comparable characteristics with the study area (Figure 4). For solar radiation, the cumulative direct solar radiation from July to October (the period not dominated by snow) as proposed by Hoelzle [1996] was used. As indicated in Figure 4, intact (active) rock glaciers that contain ice occur at high altitudes and low solar radiation while fossil rock glaciers that do not contain ice occur at low altitude and high solar radiation. The figure shows that this relationship is appropriate to distinguish between areas with and without permafrost. Guided by Figure 4, an altitude and direct solar radiation relationship was inferred for each sediment class separately (i.e., rock glaciers, LIA till, pre-LIA till, and talus). These different altitude and radiation combinations were then used and interpreted together with the results from the geophysical measurements to classify the Krummgampen catchment into areas with and without permafrost.

3.1.3. Delineation of Bedrock Surface and Spatial Distribution of Sediment Thickness

From the GPR data, the sediments that appear as horizontal reflection patterns were separated by a high-amplitude reflector from the bedrock that appears as deeply slanted reflections. Examples are shown in Figures 3a and 3b with the yellow dots indicating the bedrock surface. The identified bedrock surface was verified at locations of bedrock outcrops. For the processed seismic refraction data, compressional wave velocities above 4000 ms^{-1} were assumed to indicate bedrock. Figure 3d shows an example with the black line indicating the bedrock surface. At locations where both GPR and seismic data were available, the methods were checked for consistency.

Depth to the bedrock surface (or sediment thickness) was regionalized to the entire catchment by Ordinary

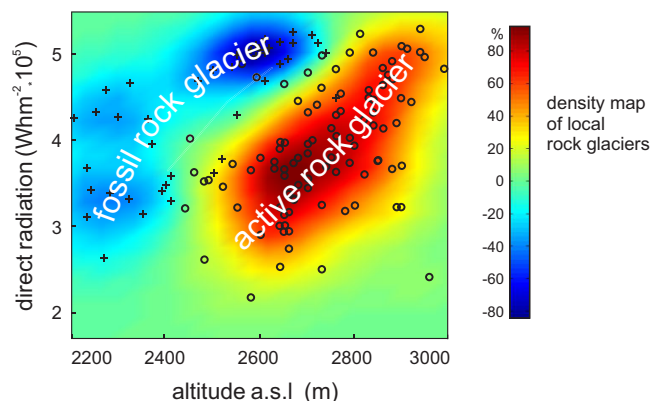


Figure 4. Direct solar radiation (July–October) versus altitude for 145 selected rock glaciers from the Tyrolean rock glacier inventory [Krainer and Ribis, 2012]. Pluses indicate fossil rock glaciers (without ice), circles indicate active (intact) rock glaciers (with ice). Background colors show a density map of the data points.

Kriging using both the GPR and seismic results. To improve the regionalization for locations far from the GPR and seismic measurements, auxiliary cross sections and points based on geomorphometric relationships were introduced. For the talus slopes, auxiliary cross sections were chosen (Figure 5a) where the sediment thickness was estimated by extending the bare rock surface below the sediment deposit through a parabola fitted to the bedrock slopes at the outcrop boundaries (Figure 5b). The parabolas were constrained by the two tangents at the deposit/bedrock margins from the DEM (1 m grid size). In cases where no

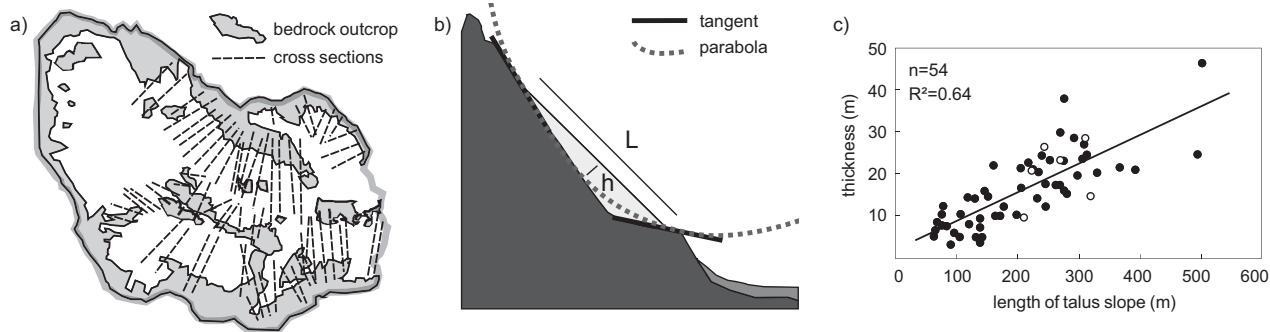


Figure 5. Examples of auxiliary cross sections and points used for the Kriging approach for talus slopes: (a) location of the auxiliary cross sections; (b) schematic cross section of bedrock (dark grey) and sediment (light grey) and parabola fitted to the two tangents at the outcrop boundaries, and (c) relationship between estimated maximum talus thickness from parabolas and length of slopes used to define additional auxiliary points for the interpolation (open circles show results of seismic measurements used to validate the relationship).

bedrock outcrop at the lower boundary existed, a horizontal tangent was used. Based on the fitted parabolas, the maximum sediment thicknesses of the talus slopes at the auxiliary cross sections were estimated and related to the length of the slopes (Figure 5c). This relationship was tested against the measured thicknesses from the seismic profiles (Figure 5c). The locations of maximum sediment thickness were used as auxiliary points for the Kriging approach. For rock glaciers, a similar correlation between the length of their front slopes and sediment thickness was used to specify auxiliary points. For the LIA and pre-LIA till deposits, no significant geomorphometric relationships were found, so mean sediment thicknesses estimated from all measured profiles were used as auxiliary points for interpolating the depth to the bedrock surface.

The depth to the permafrost table (or active layer depth) was estimated for those areas where permafrost is present. These areas were available from analysis performed in section 3.1.2. The depth to the permafrost table was estimated by a simple linear regression of the depth to the permafrost table from the seismic data with topographic altitude (Figure 6).

3.2. Results of the Geophysical Investigations

Figure 7a shows the interpolated depth to the bedrock boundary (or sediment thickness). The areas with strong increases in the sediment thickness of about 25 m are associated with landforms such as rock glaciers that are distinct morphologic features on the bedrock with steep (>30°) front and side walls. The sediment thickness gives an idea about the potential water storage capacity in the subsurface. Part of the sediment is frozen due to permafrost occurrence which constrains water flow. The depth to the permafrost table is given by the thickness of the active layer (i.e., the depth of the unfrozen sediment in Figure 7b). In total about 70% of the catchment area is underlain by permafrost and about 35% of the sediment volume is frozen.

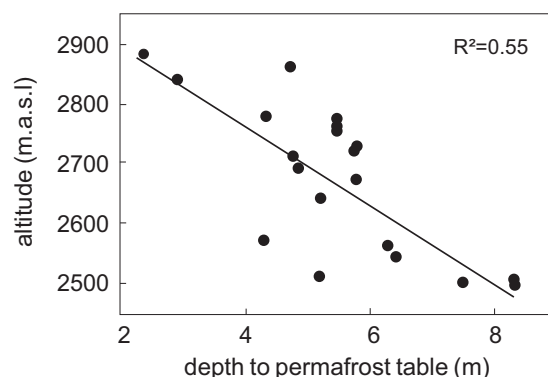


Figure 6. Linear regression between active layer depth and altitude used for estimating the active layer depth in the catchment. Points show mean active layer depths identified at seismic measurement profiles.

4. Flow Path Concepts of Unconsolidated Sediments With and Without Permafrost

In order to facilitate the hydrological modeling of the catchment, the extensive information from the field surveys (Figure 2) was used to develop flow path concepts for the different unconsolidated sediment classes in the catchment. The results from the seismic refraction measurements, the GPR profiles and the wGST measurements were interpreted for selected profiles together with the knowledge on permafrost environments reported in the literature. Information on runoff processes observed during field visits was also included. Seismic field

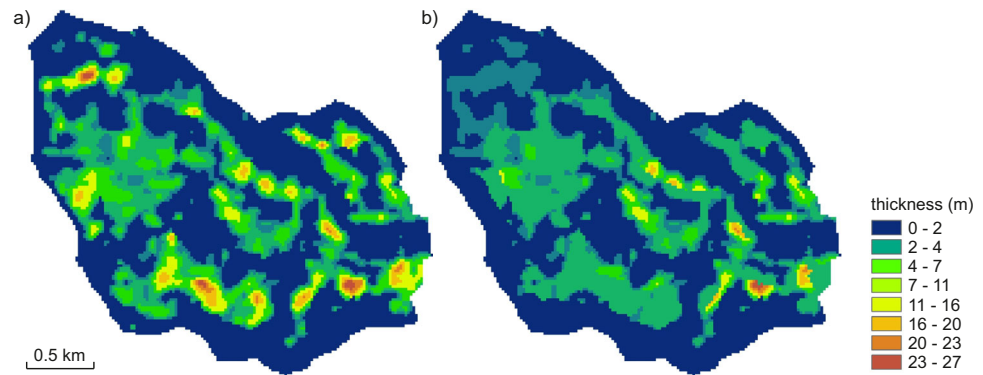


Figure 7. (a) Total sediment thickness and (b) active layer thickness, i.e., unfrozen sediment thickness due to presence of permafrost in the Krummgampen.

investigations suggest that two different types of permafrost exist in the catchment: ice-cemented permafrost bodies where ice fills the available pore space of the ground and ice-cored permafrost bodies that consist of an ice matrix with some debris or pure ice.

Below, four concepts of flow paths in talus, pre-LIA till, LIA till, and rock glaciers are presented. For the classes where field information indicated the presence of permafrost, flow paths with and without permafrost are conceptualized.

4.1. Talus

Figure 8.1a shows the results of the seismic refraction measurements at profile 11 (Figure 2), a south facing talus slope. Low compressional wave velocities in the upper layer (~ 500 m/s) indicate very coarse unfrozen material and high porosities. The velocities increase with depth to about 2000 m/s which is interpreted as a decrease in grain size and consequently in total porosity. The bedrock boundary is delineated where velocities increase to values larger than 4400 m/s and is shown as a black line in Figure 8.1a. Temperature measurements at three locations along a talus slope nearby (Figure 2) indicate very low mean winter ground surface temperatures (mean wGST $< -4^{\circ}\text{C}$) at the lowest measurement point near the toe of the slope, and the seismic refraction measurements show an increase in compressional wave velocities to around 2400 m/s which both suggest the presence of permafrost [Hauck and Kneisel, 2008]. The probable permafrost table is marked as a dashed blue line in Figure 8.1a, where velocities increase from 500 m/s to more than 2400 m/s. The occurrence of permafrost at the toe of talus slopes has been reported in several studies in the Swiss Alps [Delaloye and Lambiel, 2005; Morard et al., 2010; Phillips et al., 2009; Scapozza et al., 2011]. In these cases, permafrost occurrence was attributed to a chimney effect of air circulation in the coarse-grained talus slope causing an overcooling of the ground in the lower part of the slope. In the Krummgampen catchment, the geophysical investigations detected permafrost in the toes of south facing slopes and permafrost throughout the profiles in the north facing talus slopes. Some of the talus slopes contain ice lenses that are remains of the past glaciations, but they cover a very limited area of about 0.07 km^2 (1.3% of the catchment area) as estimated during the geological field surveys (Figure 2). The maximum sediment depth of the talus slopes is about 30 m as indicated by the seismic refraction measurements.

Figure 8.1b illustrates the inferred flow paths in a talus slope that contains an ice-cemented permafrost body in the slope toe. When permafrost is present, water from precipitation or snowmelt may infiltrate down to the bedrock in the upper parts of the profile, but only to the permafrost table in the lower parts of the profile. Because of the presence of permafrost ice which fills the pore space, the overall storage capacity of the talus slope is reduced. If permafrost disappears, the storage capacity will increase as water may percolate through the whole profile into deeper layers (down to the bedrock) and groundwater flow may occur mainly in the deeper parts of the profile. For the north facing slopes, runoff processes are similar but permafrost may occur in the entire profile reducing the storage capacity even more than in the case presented in Figure 8.1b. During the melting season, when snowpacks release large amounts of water, the authors observed exfiltration at the toe of the talus slopes resulting in extended saturation areas during several field visits in August 2010. Saturated areas might also occur when permafrost has completely disappeared, but

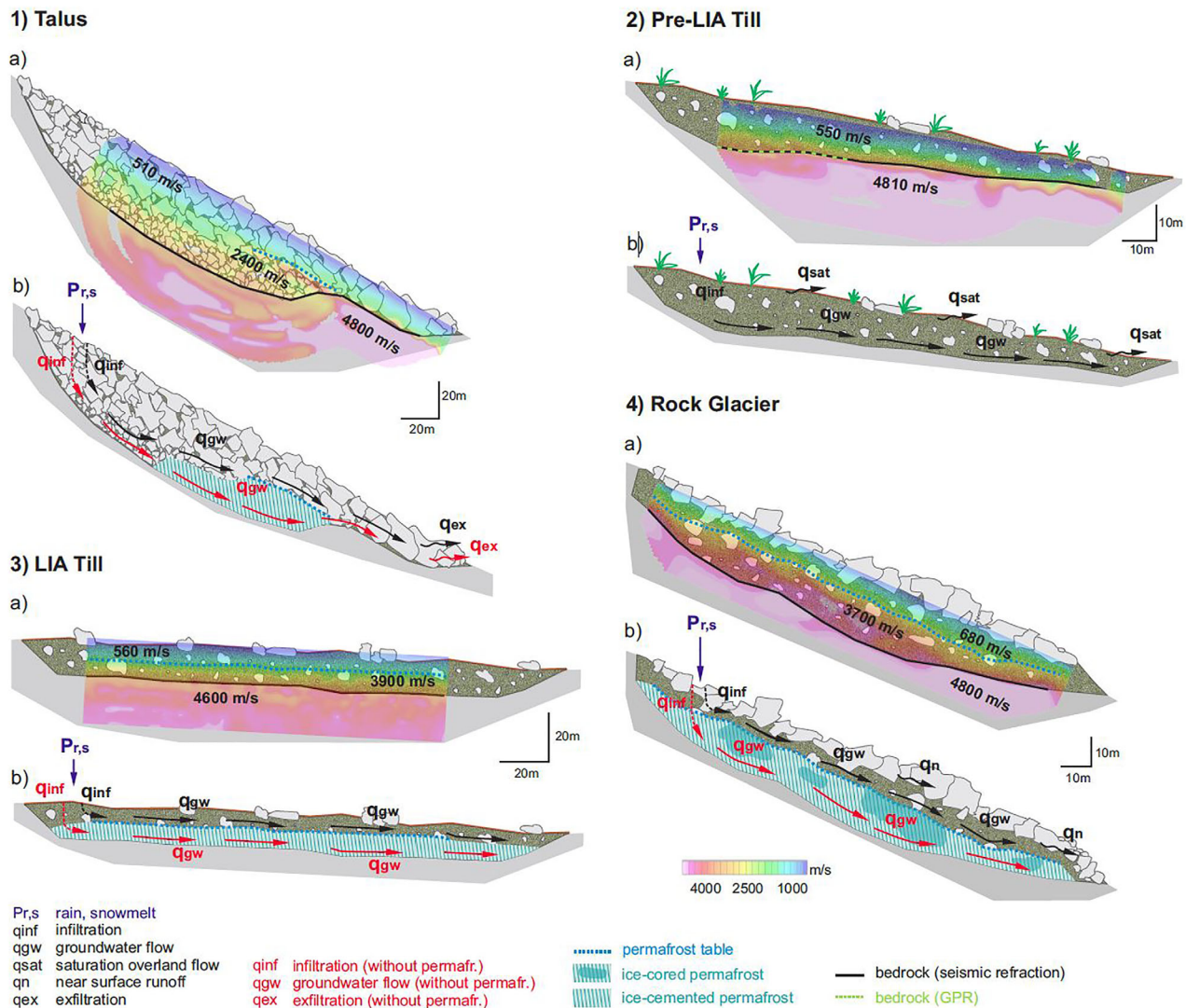


Figure 8. Flow path conceptualizations for a: (1) talus profile (profile 11), (2) pre-LIA till profile (profile 28), (3) LIA till profile (profile 26), and (4) rock glacier (profile 21). For all profiles: (a) compressional wave velocity distributions from the tomographic approach (colored); interfaces identified from GPR data are shown as dashed green line; black lines indicate interpreted bedrock surface, dashed blue lines indicate permafrost table. (b) Flow paths; black arrows refer to flow paths with permafrost, red arrows to flow paths without permafrost.

they are likely to be smaller due to the increased storage capacity of the talus slope. Surface runoff is not expected to occur on talus slopes, irrespective of the presence of permafrost, due to their large depth and hydraulic conductivity. In the presented conceptualization, it is assumed that permafrost extends down to the bedrock. Drillings on talus slopes in the Swiss Alps [Scapozza *et al.*, 2011] showed that, in some cases, permafrost does extend down to the bedrock and in others it does not, which means that some unfrozen material may be present between the permafrost and the bedrock caused by the chimney effect mentioned above. Since no borehole data were available for the Krummgampen catchment, the permafrost was assumed to always extend to the bedrock which can be interpreted as the maximum permafrost thickness to be expected.

4.2. Pre-LIA Till

Figure 8.2a shows seismic refraction measurements at pre-LIA profile 28 (Figure 2). The surface of the bedrock can be easily delineated from the measurements as compressional wave velocities increase abruptly to more than 4800 m/s at a depth of a few meters. The GPR measurements line a consistent bedrock surface (dashed green line in Figure 8.2a). Grain size analysis showed that the pre-LIA till consists of poorly sorted material and contains a high amount of fine-grained sediments. It is covered by a very thin layer of soil



Figure 9. Saturation overland flow observed on pre-LIA till during snowmelt (20 July 2009, photo: Hausmann).

(<10 cm) and vegetation. The thickness of the pre-LIA till deposits ranges from 4 m to a maximum of 8m. On this sediment type, all geophysical measurements (in total 3 GPR and 4 seismic refraction measurements) and temperature measurements (16 sensors, mean wGST between 0°C and -0.5°C) indicate the absence of permafrost. This is likely to be caused by the fact that the pre-LIA till covers the lowest elevations in the catchment (<2800 m) and is consistent with the observations that alpine permafrost is more common in areas of large grain sizes than of fine-grained materials [e.g., *Boeckli et al.*, 2012; *Scapozza et al.*, 2011]. The pre-LIA till was therefore interpreted to be permafrost free.

Figure 8.2b shows the conceptualized flow paths. Water from rainfall and snowmelt may infiltrate down to the bedrock and form a shallow groundwater flow. Due to the small thickness and high amount of fine-grained sediments, the till deposits may get saturated and produce saturation overland flow which was observed several times during the snowmelt period (see photo in Figure 9). The upper layers of the till were observed to be quite moist in early spring and summer after snowmelt suggesting that this type of sediment is usually close to saturation during spring and summer months. Hence, also summer precipitation events may cause surface runoff on areas covered with pre-LIA till.

4.3. LIA Till

The LIA till has a similar thickness as the pre-LIA till, but occurs at higher elevations (>2800 m) than the pre-LIA till, is less compact and almost free of vegetation. While no permafrost was detected for pre-LIA till, the seismic refraction measurements at LIA till profile 26 (Figure 8.3a) do indicate the presence of permafrost at depths of a few meters by a change of compressional wave velocities from 560 to 3900 m/s. The surface of the bedrock occurs at the depth where the velocity increases to more than 4400 m/s. Temperature measurements at several locations of the LIA till showed wGST between -2 and -1°C indicating possible permafrost [*Haeblerli*, 1978]. It is therefore very likely that permafrost occurs sporadically on some confined areas in the LIA till. Figure 8.3b shows the possible flow paths in the LIA till for the situation with an ice-cemented permafrost body and without permafrost. If permafrost is present, water can only infiltrate down to the permafrost table on which a shallow groundwater table evolves. Where permafrost is absent, water infiltrates down to the bedrock and groundwater flow occurs in greater depths. On this type of sediment, in contrast to the pre-LIA till, no surface runoff was observed during field trips, which suggests that the LIA till has a larger hydraulic conductivity than Pre-LIA till.

4.4. Rock Glaciers

Two types of rock glaciers exist in the catchment, intact (active) rock glaciers and fossil rock glaciers (Figure 2) which have the same structure with the only difference that fossil rock glaciers do not contain permafrost ice. The internal structure of the debris of the intact rock glacier presented in Figure 8.4a is characterized by two layers, a very coarse-grained surface layer lacking fine-grained sediment underlain by sediment with high amounts of fine-grained material. The average grain size of the surface layer is around 40 cm, but individual blocks may be as large as 2 m as observed during field visits. The lower layer is poorly sorted, mainly consisting of silty-sandy material with some larger blocks. The permafrost table was detected at a depth of approximately 4–7m where compressional wave velocities increase from 680 to 3700 m/s. The bedrock occurs at a depth where velocities increase even further to 4800 m/s. The geophysical and geological surveys suggest that the intact rock glaciers in the catchment are mainly ice-cemented rock glaciers, but a

small area of about 0.02 km² (0.5% of the catchment area) is covered by ice-cored rock glaciers that contain lenses of massive ice (Figure 2).

The flow paths shown in Figure 8.4b apply to ice-cored and ice-cemented intact rock glaciers. In the case of ice-cored rock glaciers, disappearance of permafrost will cause a subsidence of the sediment surface. For fossil rock glaciers, only the flow paths without permafrost are relevant. Flow paths in rock glaciers are generally complex. *Krainer and Mostler* [2002] showed that the water temperatures of springs located at the bottom of rock glaciers in similar settings in the Austrian Alps remained below -1.5°C throughout the year which suggests that water passing through the rock glacier is flowing in direct contact with permafrost ice. In the flow path concept presented in Figure 8.4b, water may infiltrate down to the permafrost table where a shallow groundwater table occurs. When the lower layer composed of fine-grained material becomes saturated, a near-surface runoff component may occur in the coarser surface layer of the rock glacier. This is likely to occur after snowmelt when the lower layer is saturated. When permafrost ice disappears, the thickness of the unfrozen sediment increases (>20 m) and water may infiltrate much deeper into the unfrozen ground, causing deep groundwater flow, so near-surface runoff is unlikely. Borehole investigations of rock glaciers in neighboring catchments [*Tonidandell et al.*, 2010; *Krainer et al.*, 2015] demonstrated that unfrozen sediment with high amounts of fine-grained material is present beneath the permafrost table which will allow some of the water to percolate below the permafrost body forming a slow groundwater flow component. This component is, however, likely to be very small compared to the other runoff components and is therefore not shown in the figure.

The above description of the system is consistent with the findings of *Krainer and Mostler* [2002] from several rock glaciers in the Austrian Alps. They identified a lower groundwater reservoir in the debris that produces base flow and a near-surface reservoir in the coarse material that produces quickflow which correspond to the groundwater flow and near-surface runoff components in Figure 8.4b. Their dye tracer tests indicated a flow velocity of up to more than 300 m/h in the rock glaciers which demonstrates the presence of a quickflow or near-surface runoff component.

5. Hydrological Modeling

5.1. Model Structure and Parameterization

An important motivation of this study was to understand the impact of permafrost disappearance on the runoff regime. If long observed runoff series had been available, changes could have been detected by recession analysis [e.g., *Lyon et al.*, 2009; *Lyon and Destouni*, 2010], but they were not available here. Furthermore, this does not allow for projections into the future. Therefore, a distributed hydrological model was used to represent the processes controlling runoff generation and for assessing the effect of future permafrost loss. Distributed models reported in literature often require identification of a large number of parameters [*Holländer et al.*, 2009] which is challenging, particularly in harsh, alpine environments. Thus, instead of adopting an existing model for this study, a tailor-made model was developed, building on the knowledge from the field investigations [*Chirico et al.*, 2003a; *Holländer et al.*, 2014]. The catchment was discretized into a 20 m \times 20 m grid which was deemed appropriate for representing the spatial detail obtained from the field surveys. A continuous water balance model was set up at the grid scale, coupled with a topography-based lateral connectivity model to simulate surface and subsurface flow between the grid elements. The flow connections on the hillslopes and the channels were represented by the D_{∞} algorithm [*Tarboton*, 1997] and the D8 algorithm [*O'Callaghan and Mark*, 1984; *Jenson and Domingue*, 1988], respectively.

5.1.1. Rainfall and Snow Processes

Rainfall was assumed to be uniform across the basin. The catchment is no more than 3 km across. Even though precipitation of individual storms may vary across this distance, this variability tends to get averaged out if larger time periods are considered [*Obled et al.*, 1994]. Snow accumulation and melting processes, however, were represented in a spatially distributed way in the model in order to account for the spatial variability of snowmelt due to the altitudinal range from 2400 to 3300 m.a.s.l and the different aspect of slopes. The importance of using spatially distributed snow inputs for distributed hydrological modeling of alpine catchments has been shown by *Blöschl et al.* [1991] and *Blöschl and Kirnbauer* [1992].

Table 1. Parameters of the Snow Model

Snow Parameter	Value
DDF (mm d ⁻¹ °C ⁻¹)	2.4
T _{melt} (°C)	0.5
T _s (°C)	-0.5
T _r (°C)	2.0
SCF (%)	200
RF	0.1/0.2

Precipitation P for each element was split into rain P_r and snowfall P_s depending on air temperature T_a :

$$\begin{aligned}
 P_r &= P & T_a &\geq T_r \\
 P_r &= P \frac{(T_a - T_s)}{(T_r - T_s)} & T_s &< T_a < T_r \\
 P_r &= 0 & T_a &\leq T_s \\
 P_s &= (P - P_r)SCF
 \end{aligned}
 \tag{1}$$

where T_s and T_r are the threshold temperatures for snowfall and rainfall and SCF is a snow correction factor that accounts for the snow undercatch of the precipitation gauge (see section 2.5). Snowmelt is then calculated for each element by an extended degree-day approach that takes solar radiation into account [Hock, 1999]:

$$M = \begin{cases} (DDF + RF \cdot I)(T_a - T_{melt}) & T_a > T_{melt} \\ 0 & T_a \leq T_{melt} \end{cases}
 \tag{2}$$

where M is the melt rate, DDF the degree-day factor (mm d⁻¹ °C⁻¹), RF a radiation coefficient, I the potential clear-sky solar radiation (W m⁻²), and T_{melt} the melt temperature (°C). The potential clear-sky solar radiation was calculated as a function of the solar radiation at the top of the atmosphere, atmospheric transmissivity, solar geometry, and topographic slope and aspect [Hock, 1999].

Temperature and rainfall data for the snow model at hourly intervals were available from the weather station near the catchment outlet (Figure 2). Air temperatures measured at the weather station near the catchment outlet were scaled with elevation according to regional regressions using gradients from ten temperature stations in the same region. The parameters DDF , T_{melt} , T_r , T_s , and SCF of the snowmelt model were first a priori chosen within the ranges obtained in other studies in Austria [Reszler et al., 2008; Rogger et al., 2012a,b] and then slightly adjusted against observed runoff for the calibration period 2008 (Table 1). All five parameters were assumed to be uniform across the catchment. A snow correction of 200% was found to be needed to close the water balance of the catchment. Such a high snow correction is not surprising given the large snow fall contributions and high wind speeds at the precipitation gauge and is within the range observed in other high wind speed areas [Adam and Lettenmaier, 2003; Yang et al., 2000]. The potential clear-sky radiation as input for the snow model was estimated from solar parameters [Hock, 1999] and a digital elevation model with a resolution of 20 m × 20 m. The radiation coefficient RF was obtained by calibrating the model to observed runoff with a lower value for the north facing slopes (0.1) compared to the south facing slopes (0.2) where radiation impact is assumed to be stronger. The sum of rainfall and snowmelt was used as the water input to the surface of each element of the hydrological model.

5.1.2. Evaporation

Since the alpine and nival vegetation is quite sparse in the catchment with small rooting depths, we expect transpiration to be negligible as compared to soil evaporation. The actual evaporation (E_a) is assumed to be equal to a fraction (S_E) of the potential evaporation (E_p) following, e.g., Famiglietti and Wood [1994], Simmons and Meyer [2000], and Pollacco and Mohanty [2012]. Romano and Giudici [2009] showed this method to be reliable if S_E is assumed to be the effective saturation of the sediments within a very shallow depth (D_E) of the order of a few centimeters from the terrain surface, i.e., if E_a is assumed to be equal to E_p when the sediment column is completely saturated and it linearly decreases with the effective saturation within a depth D_E . The fraction S_E is calculated as:

$$S_E = 1 - \frac{D}{D_E}(1 - S) \quad 1 \geq S \geq 1 - \frac{D_E}{D}
 \tag{3}$$

where S is the effective saturation of the sediment deposit, D_E is set to 5 cm, following Pollacco and Mohanty [2012]. Evaporation occurs only if $S > (1 - D_E/D)$, i.e., when the water table reaches the soil layer where evaporation occurs. The mean potential evapotranspiration of the catchment was calculated by the modified Blaney Criddle method [Deutscher Verband für Wasserwirtschaft und Kulturbau, 1996] as a function of air temperature and terrain.

5.1.3. Subsurface Flow Modeling

The subsurface flow model was set up in a way to represent important processes in an alpine permafrost catchment. These catchments may behave quite different compared to high-latitude permafrost catchments, in particular the seasonal variations of the active layer depth (or the occurrence of seasonal ice) may be much less pronounced. An early onset of snow in October/November in alpine catchments in Switzerland has for instance been shown to prevent soil freezing and the formation of seasonal ice [Bayard *et al.*, 2005]. In the Krummgampen catchment, snow observations at the weather station near the catchment outlet (Figure 2) showed a regular onset of a continuous snow layer in October/November so an isolating effect is expected to occur. Furthermore, ground temperature measurements at rock glaciers in nearby catchments did not indicate a seasonal ground thawing phase [Krainer and Mostler, 2004; Krainer *et al.*, 2010a, 2010b], and the seismic refraction measurements in the Krummgampen catchment (coherent waveform stacks) did not indicate the presence of seasonal ice. A strong variation in the active layer or formation of seasonal ice is therefore not expected to occur in the Krummgampen catchment. Since the lower boundary for water flow is not expected to be dynamic, an explicit representation of the vertical heterogeneity of flow processes was not deemed necessary. The sediment deposit of each catchment element was therefore modeled as a lumped water reservoir, with a downslope outgoing subsurface flow according to a nonlinear kinematic model [Sloan and Moore, 1984; Chirico *et al.*, 2003b]:

$$Q = W \cdot T(\Theta) \cdot \tan \beta \quad (4)$$

where Q is the lateral subsurface flow, W the flow width, $T(\Theta)$ the lateral transmissivity function of the relative water storage Θ expressed as the ratio of volume of stored water to the total volume of the sediment deposit, and β the element bedrock slope angle. The flow width was assumed to be equal to the grid element size, following Chirico *et al.* [2005]. The lateral transmissivity relationship to relative water storage is expected to be nonlinear with large transmissivities when the sediment deposit is close to saturation, i.e., when the large conduits within the coarser sediment layers are activated, and very low values when the available water is trapped within the finer sediments. For this reason, a combination of two power law equations is used for simulating the lateral subsurface flow [Chirico *et al.* [2005]:

$$\frac{T}{D} = K \left(\frac{\Theta - \Theta_L}{\Theta_s - \Theta_L} \right)^{\alpha_s} + M \cdot K \left(\frac{\Theta - \Theta_L}{\Theta_s - \Theta_L} \right)^{\alpha_m} \quad (5)$$

where D is the thickness of the sediment deposit, K the saturated hydraulic conductivity, Θ_L is the lower limit of the relative water storage within the sediment deposit below which subsurface flow is negligible, Θ_s the relative water storage at saturation, M an amplification factor of the conductivity close to saturation, and α_s, α_m are shape parameters, with $\alpha_m > \alpha_s$. The ratio $S = (\Theta - \Theta_L) / (\Theta_s - \Theta_L)$ is referred to as effective saturation of the sediment deposit.

In order to determine the parameters of the subsurface flow model, hydraulic conductivities were estimated based on the sediment samples using different empirical approaches [Hazen, 1892; Alyamani and Sen, 1993]. The ranges of the estimated mean hydraulic conductivities are listed in Table 2. Note that for talus no sample analysis was performed; the listed values were taken from the literature. Additionally, total porosities were estimated for each class using the results of the seismic refraction measurements and applying the empirical relationship of Watkins *et al.* [1972]:

$$\varphi = -0.175 \cdot \ln(v_p) + 1.56 \quad (6)$$

where φ is the total porosity and v_p is the compressional wave velocity. For each sediment class, a mean total porosity was estimated from a number of measured profiles (Table 2).

The parameters controlling the subsurface flow (equation (5)) were assumed to be uniform within each of the four unconsolidated sediment classes (Talus, pre-LIA till, LIA till, and intact/fossil rock glaciers), but differ between the classes. The relative water storage capacities at saturation Θ_s were assumed to be equal to the mean porosities estimated from the compressional wave velocities (Table 2). The Θ_s value for the LIA till and rock glaciers were adjusted guided by geologic experience. Geologic observations in the catchment and the region indicate that LIA till has a lower porosity than talus and rock glaciers due to the higher amount of fine-grained sediment, while rock glaciers in the catchment and in surrounding areas have been investigated in detail indicating higher-porosity values [Berger *et al.*, 2004; Hausmann *et al.*, 2012]. The lower

Table 2. Subsurface Properties From Field Investigations and Parameter Values of the Hydrologic Model for the Krummgampen Catchment

Geologic Class	Field Investigations			Subsurface Flow Model Parameters ^a				
	Hydraulic Conductivity k (mm/s)	Mean k (mm/h)	Mean Total Porosity ^b	Θ_s	K (mm/h)	α_s	α_m	M
Talus	0.017–9.4 ^c	16,950	0.42	0.42	17,000	12		0
Pre-LIA till	0.010–0.282 ^d	526	0.36	0.36	500	30		0
LIA till	0.007–0.163 ^d	306	0.43	0.38	800	30		0
Rock glacier	0.064–11 ^d	19,915	0.38	0.40	20,000	5	70	100

^aSubsurface flow model parameters used in this paper.
^bMean total porosities estimated from the seismic refraction measurements in the catchment using the equation of *Watkins et al.* [1972].
^cHydraulic conductivities values taken from literature [*Pierson, 1982; Clow et al., 2003*].
^dHydraulic conductivities estimated from grain size distribution of sediment samples in the Krummgampen catchment using different empirical approaches [*Hazen's, 1892; Alyamani and Sen, 1993*].

limit of the relative water storage Θ_L was assumed to be equal to 0.1, a representative value for very coarse grained sediments [*Romano et al., 2011*]. Rock outcrops and glacier areas were assumed impermeable, with zero storage capacity. Values of the mean hydraulic conductivity K were chosen according to the mean of the ranges estimated from sediment texture k (Table 2). Only for the LIA till class, a larger value of K was assumed, since it was formed by smaller glaciers with shorter transport distances than the pre-LIA till (resulting in less fine grained material at the base) and is therefore expected to have larger conductivities than the latter. Besides, no surface runoff was observed on LIA till during field visits, while on pre-LIA till surface runoff occurred frequently (see Figure 9) indicating a higher conductivity (and porosity) for the LIA till. Note that K values reflect the properties of the dominant sediment matrix as assessed by field observations and geophysical investigations. Local hydraulic conductivity may vary within the sediment deposits where the fraction of fine-grained sediment increases with depth. As a result, the integral transmissivity is expected to be somewhat nonlinear with respect to the relative water storage, as flow paths in layers of coarser sediments are activated only with high relative water storage, especially in the case of the rock glacier. This effect is represented by the nonlinear transmissivity law (equation (5)), with parameters α_s , α_m and M . These parameters were calibrated to the observed runoff by trial and error for the year 2008 as a calibration period (Table 2). The second component of the transmissivity law, with parameters M and α_m , was only used for the rock glaciers due to the stronger variability in their internal structure (Figure 8.4a) compared to the other sediment classes which is expected to result in a more nonlinear behavior. For the thickness of the sediment deposits (D), two scenarios were examined: (i) the depth of the active layer depth or unfrozen sediment thickness (Figure 7b) that represents the sediment layer where water can flow in the current situation with permafrost; and (ii) the total sediment thickness (Figure 7a) that represents a future scenario where permafrost has completely disappeared due to climate change.

5.1.4. Surface Flow Modeling

Given the very coarse grain-size of the deposits, it was assumed that overland flow is generated at element scale only after soil saturation by water input from direct rainfall or surface and subsurface flow from the upslope elements. The routing time of the surface flow from the elements to the outlet is

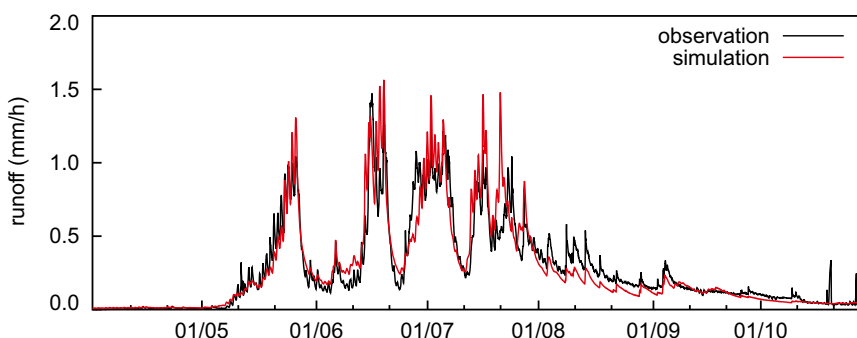


Figure 10. Observed and simulated runoff in the Krummgampen catchment at hourly resolution (April–October, 2009).

Table 3. Model Efficiencies

Year	Nash Sutcliffe Model Efficiency
2008	0.81
2009	0.89
2010	0.76
2011	0.75

expected to be generally smaller than 1 h, given the short distance and the steepness of the terrain. Since we were not interested in the runoff response at time scales smaller than 1 h and for parsimony, we routed the overland flow to the catchment outlet without any delay, following the approach proposed by *Western et al.* [1999] which does not require the specification of any parameters. All surface flow from upslope elements is infiltrated if the element is unsaturated (run-on infiltration).

5.2. Modeling Results

5.2.1. Current Situation With Permafrost

The hydrological model was used to simulate runoff in the period 2008–2011. The data from 2008 were used for calibration, those from 2009 to 2011 for validation. For the entire period, water flow was assumed to only take place in the active layer or unfrozen sediment (Figure 7b). Figure 10 shows the simulation results from April to October 2009. Runoff in the catchment is usually dominated by snowmelt processes until mid July and only in late summer/autumn runoff peaks are caused by rainfall events. The results indicate that the model is able to capture well the seasonal runoff dynamics and the water balance of the catchment. The Nash-Sutcliffe coefficients for the whole simulation period 2008–2011 are reported in Table 3 and indicate very good model performance. We are particularly interested in how well the model represents the runoff recessions as this sheds light on how well the subsurface processes (storage, subsurface routing) are represented. As can be seen in Figure 10, the recessions are captured well.

The hydrological behavior of the different unconsolidated sediment classes according to the flow path conceptualizations proposed in section 4 was visualized by saturation maps for different time slices. Figure 11 shows two examples. The distribution of saturation is consistent with the understanding of the hydrological functioning of the catchment from the field visits and flow path concepts. Talus slopes for instance are never completely saturated due to their very high hydraulic conductivities, neither during runoff events in summer (Figure 11a) nor during the low flow period in autumn (Figure 11b). Intact rock glaciers on the other hand can get saturated during the snowmelt period and during summer as illustrated in Figure 11a. Toward autumn, saturation decreases (Figure 11b). During the field visits in summer, running water was indeed audible in the coarse layer of the intact rock glaciers. Fossil rock glaciers are unsaturated throughout the year due to their large thickness of unfrozen sediment. LIA till is almost saturated during the summer flood events and saturation decreases toward the low flow period in autumn. This is in accordance with the fact that no surface runoff was observed on LIA till during the field visits. The LIA till areas that appear to be saturated in the figure are those with a very low sediment thickness. pre-LIA till areas are almost completely saturated during the summer flood event and parts of the areas remain saturated even during the low flow period. This is because pre-LIA till has a lower hydraulic conductivity than the LIA till and surface runoff was often observed on these areas.

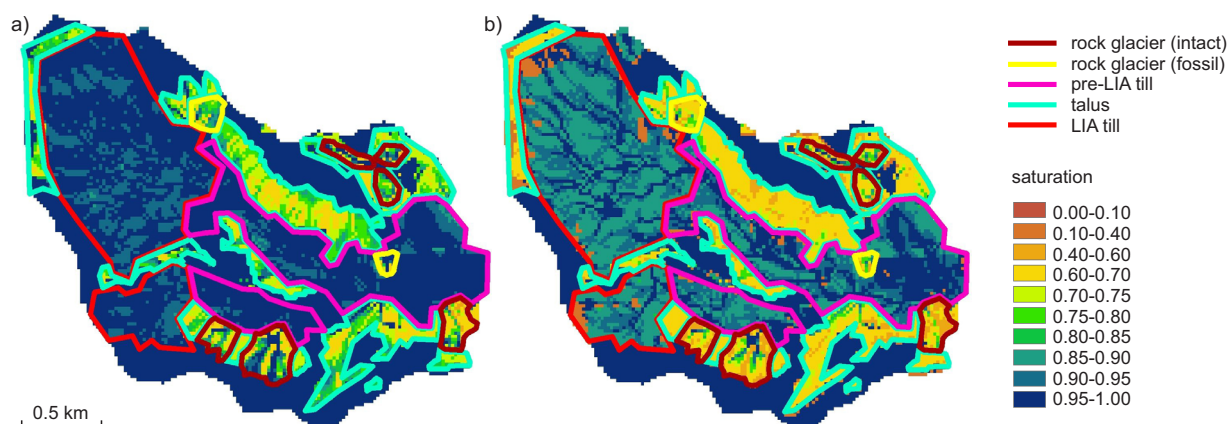


Figure 11. Maps of degree of saturation of the unfrozen sediment during (a) a runoff event in summer (12 August 2010) and (b) a low flow period in autumn (1 October 2008) in the Krummgampen catchment. Unconsolidated sediment classes are indicated by colored lines.

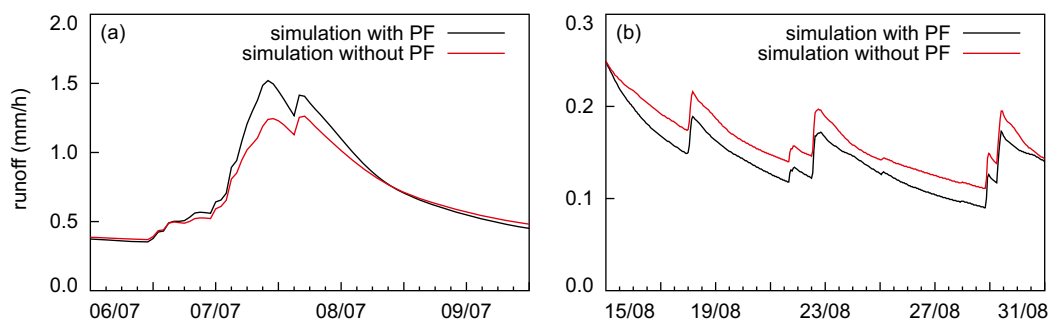


Figure 12. Changes in runoff due to permafrost (PF) thawing; (a) a summer event in July 2008 and (b) recession period in late August 2009. Black line shows current situation with permafrost, red line shows scenario without permafrost.

5.2.2. Scenario Without Permafrost

In order to assess the hydrological effects of a potential situation where permafrost has completely disappeared in a warmer climate, a scenario without permafrost was run using the input data for 2008–2011, but the lower boundary for water flow was assumed to be the surface of the bedrock for all geologic classes (Figure 7a). The parameters of the unconsolidated sediment classes were assumed to be the same as for the current situation (Table 2). Seismic data indicate that most sediments are not oversaturated with ice, but that the ice fills the pore space between the grains. Therefore, porosities and also hydraulic conductivities are not expected to change significantly when the permafrost disappears. Some of the talus slopes and rock glaciers contain ice lenses which would probably result in some subsidence when the lenses melt. This effect was neglected in the model since it only occurs in about 2% of the catchment area and does not influence the sediment properties.

The simulation results suggest that the flood peaks decrease substantially when all the permafrost ice disappears. A comparison of the two largest floods of each year in the two scenarios shows a decrease in the peak runoff between 7 and 17%. This reduction occurs because of the increase in thickness of unfrozen sediment when permafrost disappears which results in a larger volume of water infiltrating in the sediment deposits. This in turn reduces the surface runoff and consequently the flood peaks. The differences in the reduction of the flood peak can be attributed to the differences in antecedent soil moisture. An example for such a decrease for a flood event in summer 2008 is shown in Figure 12a. The change mainly occurs for the flood peak volume most likely due to the smaller extent of saturation areas when permafrost is absent. During the recession period, there is an increase in runoff, as illustrated for the late August 2009 in Figure 12b. The scenario indicates an increase in monthly runoff in August, September and October between 1 and 19%. This increase is consistent with the decrease in the flood peaks as more water will infiltrate due to the increase in subsurface storage and flow through the subsurface due to the larger cross-sectional area.

6. Discussion

6.1. Flow Path Concepts

The paper presents flow path concepts derived from geophysical measurements for four sediment types in a high alpine catchment influenced by permafrost. For the till deposits, for instance, two main flow paths have been identified: a shallow groundwater flow on the surface of the permafrost table for places where permafrost is present and a deeper groundwater flow over bedrock at unfrozen locations. These flow paths are similar to those found by *McClymont et al.* [2011] in a proglacial moraine (till): shallow groundwater flow over margins of buried ice, deeper groundwater flow through the moraine over bedrock and possibly very deep groundwater flow paths through a network of fractures within the bedrock. The geology of the Krummgampen catchment suggests that the third flow path through fractures in the bedrock does not exist or is insignificant. Geophysical investigations identified permafrost in the toes of the talus slopes which has also been reported from other locations in the Alps [*Delaloye and Lambiel, 2005; Morard et al., 2010; Phillips et al., 2009; Scapozza et al., 2011*]. In some north-facing talus slopes of the Krummgampen catchment, permafrost was even present along the entire profile. Flow through these talus slopes always occurs as deep groundwater flow due to their great thickness and large hydraulic conductivities but, when permafrost is present, the lower boundary of the groundwater flow is the permafrost table which means that the storage

capacity of the talus slope is reduced. This is important because talus slopes have been shown to significantly influence runoff generation of alpine catchments by their storage behavior [Clow *et al.*, 2003; McClymont *et al.*, 2010; Liu *et al.*, 2004] which is smaller when permafrost is present. The flow paths of rock glaciers show two main pathways: a groundwater flow in the lower layer that is composed of finer-grained material and a near-surface runoff component in the coarser-grained upper layer when the lower layer is saturated. These pathways are consistent with the two storage reservoirs identified by Krainer and Mostler [2002] in similar rock glaciers in the region.

6.2. Runoff Model Parameterization

The flow path concepts have been used to parameterize a spatially distributed hydrological model. In the process of setting up the model it became clear that the understanding of the flow paths for the different sediment types as well as the other information from the field surveys were extremely helpful in selecting realistic values of the model parameters. The geophysical data on the subsurface were especially valuable but other, less quantitative information such as observations of the presence of surface saturation (e.g. Figure 9) was also very useful. In identifying model parameters, the value of field observations is sometimes not fully appreciated in the literature [Grayson and Blöschl, 2000]. It is true that the parameters cannot be measured for each and every model element, but the range of possible parameter values can be much constrained by different field data such as those obtained in this study. Indeed, only a few parameters had to be adjusted by comparing the runoff simulations with the observed hydrographs and the adjustments were small. This is in stark contrast to the notion of equifinality proposed in the literature [Beven, 2006]. While there is an element of indeterminism in the model parameters, this study suggests that it may be more helpful to go to the field and measure the subsurface characteristics, and observe runoff processes, instead of running a large number of model simulations to explore the possible parameter space on the basis of runoff data alone. This need is particularly acute in the presence of environmental change as model parameters are likely to change too, so calibration to runoff alone may not suffice in the future [Merz *et al.*, 2011; Peel and Blöschl, 2011].

6.3. Hydrological Effects of Permafrost Disappearance

The spatially distributed hydrological model was used to assess the effect of complete permafrost disappearance on the runoff dynamics. The simulation results show that flood peaks may decrease by up to 17% when the permafrost disappears. This is because the thickness of unfrozen sediment increases causing a larger storage capacity which, in turn, leads to less frequent and less extensive surface saturation and consequently to less frequent and less extensive surface runoff. This finding is consistent with the results of McNamara *et al.* [1998] who emphasized the role of permafrost in increasing the extent of saturated areas and consequently enhancing the peakiness of storm hydrographs. A second effect of permafrost disappearance in the Krummgampen catchment will be an increase of runoff during recession periods in the late summer and early autumn months of up to 19%. A similar change in runoff during recession was observed in northern Sweden due to permafrost thawing and was related to permafrost thawing rates [Lyon *et al.*, 2009]. In another study, Lyon and Destouni [2010] showed that permafrost thawing may increase the annual groundwater flow and the runoff during recession, again consistent with the findings of this study. Of course, the magnitude of the identified changes is subjected to the uncertainties involved in the estimation of the permafrost distribution and active layer depth, besides the model structure and parameters. However, the direction of change, e.g., reduction of flood peaks and increase of runoff during the recession period due to the larger storage capacity of the catchment is expected to remain the same. The change in storage capacity will have important implications for flood frequency characteristics of mountain catchments that exhibit permafrost. Rogger *et al.* [2012a, 2012b] pointed out that the shape of the flood frequency curve in mountain catchments may be controlled by the spatial distribution of the sediment storage. As thawing of permafrost ice will change the catchment storage capacity, it is likely that the shape of the flood frequency curve will also change.

7. Conclusions

The main conclusions of this paper are as follows: (a) typical flow paths exist for different types of sediments in the Krummgampen catchment which may be applicable to similar environments exhibiting mountain permafrost. Four concepts were developed in this study for talus fans, Little Ice Age (LIA) till, pre-LIA till, and

rock glaciers. These flow paths are likely to change with the thawing of permafrost. If permafrost is present, water can only infiltrate down to the permafrost table which forms the lower boundary for subsurface flow. Without permafrost, this boundary will be located deeper, i.e., at the sediment—bedrock interface. This will increase the thickness of unfrozen sediments and its storage capacity. (b) The flow path concepts inferred from the field data and more qualitative information from the field surveys were extremely helpful in selecting the runoff model structure and the model parameters. The geophysical data on the subsurface were especially valuable but other, less quantitative information such as observations of the presence of surface saturation was also very useful. It is suggested that field observations should be given a higher priority in runoff modeling than the current paradigm of using runoff alone and exploring the parameter space randomly. (c) The simulations indicate that the disappearance of permafrost ice in the Krummgampen catchment may cause a decrease in flood peak runoff of up to 17% and an increase of runoff during recession periods of up to 19%. Both changes are due to an increase in the storage capacity of the sediments in the catchment. It is anticipated that the type of combined process and modeling studies presented in this paper will gain more momentum in the future as the focus in hydrology shifts toward exploring the effects of environmental change.

Acknowledgments

We would like to acknowledge the financial support from the Austrian Academy of Sciences (ISDR-Projects “Permafrost in Austria - PART I” and “The Impact of Climate Change on Alpine Permafrost”), the Austrian Science Funds FWF (Doctoral Programme on Water Resource Systems DK-plus W1219-N22 and project P 23723-N21), and the ERC Flood Change Project (ERC advanced grant, 291152). We would also like to thank the TIWAG, Tiroler Wasserkraftwerke AG, for providing meteorological data from nearby weather stations. The data for the study are available upon request to the authors.

References

- Adam, J. C., and D. P. Lettenmaier (2003), Adjustment of global gridded precipitation for systematic bias, *J. Geophys. Res.*, *108*(D8), 4257, doi:10.1029/2002JD002499.
- Adler, S., et al. (2015), *Das Klima von Tirol - Südtirol - Belluno*, Zent. für Meteorol. und Geodyn., 109 pp., Vienna.
- Alyamani, M. S., and Z. Sen (1993), Determination of hydraulic conductivity from grain-size distribution curves, *Ground Water*, *31*, 551–555.
- Anisimov, O., and S. Reneva (2006), Permafrost and changing climate: The Russian perspective, *Ambio*, *35*, 169–175.
- Barry, R. G., and T. Y. Gan (2011), *The Global Cryosphere: Past, Present and Future*, Cambridge Univ. Press, 472 pp., New York.
- Bayard, D., M. Stähli, A. Parriaux, and H. Flüeler (2005), The influence of seasonally frozen soil on the snowmelt runoff at two Alpine sites in southern Switzerland, *J. Hydrol.*, *309*(1), 66–84.
- Berger, J., K. Krainer, and W. Mostler (2004), Dynamics of an active rock glacier (Ötztal Alps, Austria), *Quat. Res.*, *62*(3), 233–242, doi:10.1016/j.yqres.2004.07.002.
- Beven, K. (2006), A manifesto for the equifinality thesis, *J. Hydrol.*, *320*(1–2), 18–36, doi:10.1016/j.jhydrol.2005.07.007.
- Blöschl, G., and R. Kirnbauer (1992), An analysis of snow cover patterns in a small Alpine catchment, *Hydrol. Processes*, *6*, 99–109.
- Blöschl, G., D. Gutknecht, and R. Kirnbauer (1991), Distributed snowmelt simulations in an Alpine catchment: 2. Parameter study and model predictions, *Water Resour. Res.*, *27*, 3181–3188.
- BMLFUW (2005), *Hydrologischer Atlas Österreichs* [Hydrological Atlas of Austria], Bundesministerium für Land- und Forstwirtschaft, Umwelt und Wasserwirtschaft, Vienna.
- Boeckli, L., A. Brenning, S. Gruber, and J. Noetzli (2012), A statistical approach to modelling permafrost distribution in the European Alps or similar mountain ranges, *Cryosphere*, *6*, 125–140, doi:10.5194/tc-6-125-2012.
- Campbell, D. H., D. W. Clow, G. P. Ingersoll, M. A. Mast, N. E. Spahr, and J. T. Turk (1995), Processes controlling the chemistry of two snowmelt-dominated streams in the Rocky Mountains, *Water Resour. Res.*, *35*, 2811–2821.
- Chirico, G. B., R. B. Grayson, and A. W. Western (2003a), A downward approach to identifying the structure and parameters of a process-based model for a small experimental catchment, *Hydrol. Processes*, *17*, 2239–2258, doi:10.1002/hyp.1330.
- Chirico, G. B., R. B. Grayson, and A. W. Western (2003b), On the computation of the quasi-dynamic wetness index with multiple-flow-direction algorithms, *Water Resour. Res.*, *39*(5), 1115, doi:10.1029/2002WR001754.
- Chirico, G. B., A. W. Western, R. B. Grayson, and B. Blöschl (2005), On the definition of the flow width for calculating specific catchment area patterns from gridded elevation data, *Hydrol. Processes*, *19*, 2539–2556.
- Clow, D. W., L. Schrott, R. Webb, D. H. Campbell, A. Torizzo, and M. Dorblaser (2003), Ground water occurrence and contributions to streamflow in an alpine catchment, Colorado Front range, *Ground Water*, *41*, 937–950.
- Cremonese, E., et al. (2011), An inventory of permafrost evidence for the European Alps, *Cryosphere*, *5*, 651–657.
- Degenhardt, J. J., and J. R. Giardino (2003), Subsurface investigation of a rock glacier using ground-penetrating radar: Implications for locating stored water on Mars, *J. Geophys. Res.*, *108*(E4), 8036, doi:10.1029/2002JE001888.
- Delaloye, R., and C. Lambiel (2005), Evidence of winter ascending air circulation throughout talus slopes and rock glaciers situated in the lower belt of alpine discontinuous permafrost (Swiss Alps), *Norw. J. Geogr.*, *59*, 194–203.
- Draebing, D., and M. Krautblatter (2012), P-wave velocity changes in freezing hard low-porosity rocks: A laboratory-based time-average model, *Cryosphere*, *6*, 1163–1174, doi:10.5194/tc-6-1163-2012.
- Deutscher Verband für Wasserwirtschaft und Kulturbau (1996), Ermittlung der verdunstung von land- und wasserflächen, *DVWK-Merkblätter* 238, Bonn, Germany.
- Evans, S. G., S. Ge, and S. Liang (2015), Analysis of groundwater flow in mountainous, headwater catchments with permafrost, *Water Resour. Res.*, *51*, 9564–9576, doi:10.1002/2015WR017732.
- Famiglietti, J. S., and E. F. Wood (1994), Multiscale modeling of spatially variable water and energy balance processes, *Water Resour. Res.*, *30*, 3061–3078.
- Frampton, A., S. Painter, S. W. Lyon, and G. Destouni (2011), Non-isothermal, three-phase simulations of near-surface flows in a model permafrost system under seasonal variability and climate change, *J. Hydrol.*, *403*(3–4), 352–359, doi:10.1016/j.jhydrol.2011.04.010.
- Gardner, L. W. (1939), An areal plan for mapping subsurface structure by refraction shooting, *Geophysics*, *4*, 247–259.
- Gärtner-Roer, I., H. H. Christiansen, B. Etzelmüller, H. Farbröt, S. Gruber, K. Isaksen, A. Kellerer-Pirklbauer, K. Krainer, and J. Noetzli (2010), Primary impacts of climate change on the cryosphere—Permafrost, in *Impacts of Climate Change on Snow, Ice, and Permafrost in Europe*:

- Observed Trends, Future Projections, and Socioeconomic Relevance, Technical Paper, vol. 13, edited by T. Voigt et al., pp. 66–76, Eur. Environ. Agency, Copenhagen.
- Grayson, R., and G. Blöschl (Eds.) (2000), *Spatial Patterns in Catchment Hydrology: Observations and Modelling*, Cambridge Univ. Press, Cambridge, U. K.
- Haerberli, W. (1973), Die Basis-Temperatur der winterlichen Schneedecke als möglicher Indikator für die Verbreitung von Permafrost in den Alpen, *Zeitschrift für Gletscherkunde und Glazialgeologie*, *9*, 221–227.
- Haerberli, W. (1975), Untersuchungen zur Verbreitung von Permafrost zwischen Flüelapass und Piz Grialetsch (GR), *Mitteilungen der Versuchsanstalt für Wasserbau, Hydrologie und Glaziologie*, *17*, 221 pp., ETH-Zürich, Zürich, Switzerland.
- Haerberli, W. (1978), Special aspects of high mountain permafrost methodology and zonation in the Alps, in *Proceedings of the Third International Conference on Permafrost*, pp. 378–384, Natl. Res. Council of Can., Ottawa, Canada.
- Haerberli, W., C. Guodong, A. P. Gorbunov, and S. A. Harris (1993), Mountain permafrost and climatic change, *Permafrost Periglacial Processes*, *4*, 165–174.
- Harris, C., D. Vonder Mühl, K. Isaksen, W. Haerberli, J. L. Sollid, L. King, P. Holmlund, F. Dramis, M. Guglielmin, and D. Palacios (2003), Warming permafrost in European mountains, *Global Planet. Change*, *30*(3–4), 215–225, doi:10.1016/j.gloplacha.2003.04.001.
- Hauck, C., and C. Kneisel (2008), *Applied Geophysics in Periglacial Environments*, 256 pp., Cambridge Univ. Press, New York.
- Hausmann, H., and M. Behm (2011), Imaging the structure of cave ice by ground-penetrating radar, *Cryosphere*, *5*, 329–340, doi:10.5194/tc-5-329-2011.
- Hausmann, H., K. Krainer, E. Brückl, and W. Mostler (2006), Creep of two Alpine rock glaciers—Observation and modelling (Ötztal- and Stubai Alps, Austria), in *Proceedings of the 9th International Symposium on High Mountain Remote Sensing Cartography (Grazer Schriften der Geographie und Raumforschung)*, vol. 43, pp. 146–150, Inst. of Geogr. and Reg. Sci., Univ. of Graz, Graz, Austria.
- Hausmann, H., K. Krainer, E. Brückl, and W. Mostler (2007), Internal structure and ice content of Reichenkar Rock Glacier (Stubai Alps, Austria) assessed by geophysical investigations, *Permafrost Periglacial Processes*, *18*, 351–367, doi: 10.1002/ppp.60.
- Hausmann, H., K. Krainer, E. Brückl, and C. Ullrich (2012), Internal structure, ice content and dynamics of Ölgrube and Kaiserberg rock glaciers (Ötztal Alps, Austria) determined from geophysical surveys, *Aust. J. Earth Sci.*, *105*(2), 12–31.
- Hazen, A. (1892), Some physical properties of sand and gravel, with special reference to their use in filtration, 24th Annual Report, *Rep.* 34, Mass. State Board of Health, Boston.
- Hilbich, C. (2010), Time-lapse refraction seismic tomography for the detection of ground ice degradation, *Cryosphere*, *4*, 243–259.
- Hinzman, L. D., et al. (2005), Evidence and implications of recent climate change in Northern Alaska and Other Arctic Regions, *Clim. Change*, *72*, 251–298.
- Hock, R. (1999), A distributed temperature index ice and snow melt model including potential direct solar radiation, *J. Glaciol.*, *45*(149), 101–111.
- Hoelzle, M. (1992), Permafrost occurrence from BTS measurements and climatic parameters in the Eastern Swiss Alps, *Permafrost Periglacial Processes*, *3*, 143–147, doi:10.1002/ppp.3430030212.
- Hoelzle, M. (1996), Mapping and modelling of mountain permafrost distribution in the Alps, *Norw. J. Geogr.*, *50*, 11–15, doi:10.1080/00291959608552347.
- Hole, J. A. (1992), Nonlinear high-resolution three-dimensional seismic travel time tomography, *J. Geophys. Res.*, *97*, 6553–6562, doi: 10.1029/92JB00235.
- Holländer, H. M., et al. (2009), Comparative predictions of discharge from an artificial catchment (Chicken Creek) using sparse data, *Hydrol. Earth Syst. Sci.*, *13*, 2069–2094, doi:10.5194/hess-13-2069-2009.
- Holländer, H. M., et al. (2014), Impact of modellers' decisions on hydrological a priori predictions, *Hydrol. Earth Syst. Sci.*, *18*, 2065–2085, doi: 10.5194/hess-18-2065-2014.
- Ikeda, A. (2006), Combination of conventional geophysical methods for sounding the composition of rock glaciers in the Swiss Alps, *Permafrost Periglacial Processes*, *17*, 35–48, doi:10.1002/ppp.550.
- Jenson, S. K., and J. O. Domingue (1988), Extracting topographic structure from digital elevation data for geographic information system analysis, *Photogramm. Eng. Remote Sens.*, *54*(11), 1593–1600.
- Julian, A., and J. Chueca (2007), Permafrost distribution from BTS measurements (Sierra de Telera, Central Pyrenees, Spain): Assessing the importance of solar radiation in a mid-elevation shaded mountainous area, *Permafrost Periglacial Processes*, *18*, 137–149, doi:10.1002/ppp.576.
- Koch, J. C., S. A. Ewing, R. Striegl, and D. M. McKnight (2013), Rapid runoff via shallow throughflow and deeper preferential flow in a boreal catchment underlain by frozen silt (Alaska, USA), *Hydrogeol. J.*, *21*(1), 93–106.
- King, L. (1984), High mountain permafrost in Scandinavia, in *Proceedings of the 4th International Conference on Permafrost*, vol. 2, pp. 612–661, Natl. Academy Press, Washington, D. C.
- Krainer, K., and W. Mostler (2002), Hydrology of active rock glaciers: Examples from the Austrian Alps, *Arctic Antarct. Alpine Res.*, *34*(2), 142–149.
- Krainer, K., and W. Mostler (2004), Aufbau und Entstehung des aktiven Blockgletschers im Sulzkar, westliche Stubai Alpen (Tirol) (Structure and genesis of the Sulzkar rock glacier in the Stubai Alps), *Geo.Alp.*, *1*, 37–55.
- Krainer, K., and M. Ribis (2012), A rock glacier inventory of the Tyrolean Alps (Austria), *Aust. J. Earth Sci.*, *105*(2), 32–47.
- Krainer, K., K. Lang, and H. Hausmann (2010a), Active rock glaciers at Croda Rossa/Hohe Gaisl, Eastern Dolomites (Alto Adige/South Tyrol, Northern Italy), *Geogr. Fis. Dinamica Quat.*, *33*, 25–36.
- Krainer, K., P. Ausserer, D. Bressan, T. Fontana, K. Lang, and L. Mussner (2010b), Permafrostuntersuchungen in ausgewählten Gebieten Südtirols (Permafrost investigations at selected sites in Sout Tyrol), *Innsbrucker Geogr. Stud.*, *37*, 25–87.
- Krainer, K., A. Kellerer-Pirklbauer, V. Kaufmann, G.-K. Lieb, L. Schrott, and H. Hausmann (2012a), Editorial: Permafrost Research in Austria: History and recent advances, *Aust. J. Earth Sci.*, *105*(2), 2–11.
- Krainer, K., L. Mussner, M. Behm, and H. Hausmann (2012b), Multi-disciplinary investigation of an active rock glacier in the Sella Group (Dolomites; Northern Italy), *Aust. J. Earth Sci.*, *105*(2), 48–62.
- Krainer, K., et al. (2015), A 10,300-year-old permafrost core from the active rock glacier Lazaun, southern Ötztal Alps (South Tyrol, northern Italy), *Quat. Res.*, *83*, 324–335.
- Landmark Graphics Corporation (1998), *ProMAX 2D Seismic Processing and Analysis, 626075 Rev. B*, Landmark Graphics Corporation.
- Langston, G., L. R. Bentley, M. Hayashi, A. McClymont, and A. Pidlisceky (2011), Internal structure and hydrological functions of an alpine proglacial moraine, *Hydrol. Processes*, *25*, 2967–2982, doi:10.1002/hyp.8144.
- Leopold, M., M. W. Williams, N. Caine, J. Völkel, and D. Dethier (2011), Internal structure of the Green Lake 5 rock glacier, Colorado Front Range, USA, *Permafrost Periglacial Processes*, *22*, 107–119, doi:10.1002/ppp.706.

- Liu, F., M. W. Williams, and N. Caine (2004), Source waters and flow paths in an alpine catchment, Colorado Front Range, United States, *Water Resour. Res.*, *40*, W09401, doi:10.1029/2004WR003076.
- Lugon, R., and R. Delaloye (2001), Modelling alpine permafrost distribution, Val de Rechy, Valais Alps (Switzerland), *Norw. J. Geogr.*, *55*(4), 224–229, doi:10.1080/00291950152746568.
- Lyon, S. W., and G. Destouni (2010), Changes in catchment-scale recession flow properties in response to permafrost thawing in the Yukon River Basin, *Int. J. Climatol.*, *30*, 2138–2145, doi:10.1002/joc.1993.
- Lyon, S. W., G. Destouni, R. Giesler, C. Humborg, M. Mörth, J. Seibert, J. Karlsson, and P. A. Troch (2009), Estimation of permafrost thawing rates in a sub-arctic catchment using recession flow analysis, *Hydrol. Earth Syst. Sci.*, *13*, 595–604, doi:10.5194/hess-13-595-2009.
- Maurer, H., and C. Hauck (2007), Geophysical imaging of alpine rock glaciers, *J. Glaciol.*, *53*, 110–120.
- McClymont, A. F., M. Hayashi, L. R. Bentley, D. Muir, and E. Ernst (2010), Groundwater flow and storage within an alpine meadow-talus complex, *Hydrol. Earth Syst. Sci.*, *14*, 859–872, doi:10.5194/hess-14-859-2010.
- McClymont, A. F., J. W. Roy, M. Hayashi, L. R. Bentley, H. Maurer, and G. Langston (2011), Investigating groundwater flow paths within proglacial moraine using multiple geophysical methods, *J. Hydrol.*, *399*(1–2), 57–69, doi:10.1016/j.jhydrol.2010.12.036.
- McNamara, J. P., D. L. Kane, and L. D. Hinzman (1998), An analysis of streamflow hydrology in the Kuparuk River Basin, Arctic Alaska: A nested watershed approach, *J. Hydrol.*, *206*(1–2), 39–57, doi:10.1016/S0022-1694(98)00083-3.
- Merz, R., J. Parajka, and G. Blöschl (2011), Time stability of catchment model parameters: Implications for climate impact analyses, *Water Resour. Res.*, *47*, W02531, doi:10.1029/2010WR009505.
- Monnier, S., C. Camerlynck, F. Rejiba, C. Kinnard, T. Feuillet, and A. Dhemaied (2011), Structure and genesis of the Thabor rock glacier (Northern French Alps) determined from morphological and ground-penetrating radar surveys, *Geomorphology*, *134*(3–4), 269–279, doi:10.1016/j.geomorph.2011.07.004.
- Morard, S., R. Delaloye, and C. Lambiel (2010), Pluriannual thermal behaviour of low elevation cold talus slopes in western Switzerland, *Geogr. Helv.*, *65*, 124–134.
- Musil, M., H. Maurer, A. G. Green, H. Horstmeyer, F. O. Nitsche, D. Vonder Mühl, and S. Springman (2002), Shallow seismic surveying of an Alpine rock glacier, *Geophysics*, *67*, 1701–1710.
- Nelson, F. E. (2003), Geocryology: Enhanced: (Un)frozen in time, *Science*, *299*, 1673–1675.
- Nespor, V., and B. Sevruck (1999), Estimation of wind-induced error of rainfall gauge measurements using a numerical simulation, *J. Atmos. Oceanic Technol.*, *16*, 450–464.
- Oble, C., J. Wendling, and K. Beven (1994), The sensitivity of hydrological models to spatial rainfall patterns: An evaluation using observed data, *J. Hydrol.*, *159*(1–4), 305–333.
- O'Callaghan, J. F., and D. M. Mark (1984), The extraction of drainage networks from digital elevation data, *Comput. Vision Graphics Image Process.*, *28*(3), 323–344.
- Palmer, D. (1980), *The Generalized Reciprocal Method of Seismic Refraction Interpretation*, Soc. of Explor. Geophys., Tulsa, Okla.
- Peel, M. C., and G. Blöschl (2011), Hydrologic modelling in a changing world, *Prog. Phys. Geogr.*, *35*(2), 249–261.
- Phillips, M., E. Zenklusen Mutter, M. Kern-Luetsch, and M. Lehning (2009), Rapid degradation of ground ice in a ventilated talus slope: Flüela Pass, Swiss Alps, *Permafrost Periglacial Processes*, *20*, 1–14, doi:10.1002/ppp.638.
- Pierson, T. C. (1982), Classification and hydrological characteristics of scree slope deposits in the Northern Craigieburn Range, *J. Hydrol.*, *21*(1), 34–59, New Zealand.
- Pollacco, J. A. P., and B. P. Mohanty (2012), Uncertainties of water fluxes in SVAT models: Inverting surface soil moisture and evapotranspiration retrieved from remote sensing, *Vadose Zone J.*, *11*(3), doi:10.2136/vzj2011.0167.
- Reszler, Ch., J. Komma, G. Blöschl, and D. Gutknecht (2008), Dominante Prozesse und Ereignistypen zur Plausibilisierung flächendetailierter Niederschlag-Abflussmodelle [Dominant processes and event types for checking the plausibility of spatially distributed runoff models], *Hydrol. Wasserbewirtschaftung*, *52*(3), 120–131.
- Rogger, M., B. Kohl, H. Pirkl, A. Viglione, J. Komma, R. Kirnbauer, R. Merz, and G. Blöschl (2012a), Runoff models and flood frequency statistics for design flood estimation in Austria—Do they tell a consistent story?, *J. Hydrol.*, *456–457*, 30–43, doi:10.1016/j.jhydrol.2012.05.068.
- Rogger, M., H. Pirkl, A. Viglione, J. Komma, B. Kohl, R. Kirnbauer, R. Merz, and G. Blöschl (2012b), Step changes in the flood frequency curve: Process controls, *Water Resour. Res.*, *48*, W05544, doi:10.1029/2011WR011187.
- Romano, E., and M. Giudici (2009), On the use of meteorological data to assess the evaporation from a bare soil, *J. Hydrol.*, *372*(1), 30–40.
- Romano, N., M. Palladino, and G. B. Chirico (2011), Parameterization of a bucket model for soil-vegetation-atmosphere modeling under seasonal climatic regimes, *Hydrol. Earth Syst. Sci.*, *15*, 3877–3893, doi:10.5194/hess-15-3877-2011.
- Romanovsky, V. E., et al. (2010), Thermal state of permafrost in Russia, *Permafrost Periglacial Processes*, *21*(2), 136–155, doi:10.1002/ppp.683.
- Scapozza, C., C. Lambiel, L. Baron, L. Marescot, and E. Reynard (2011), Internal structure and permafrost distribution in two alpine periglacial talus slopes, Valais, Swiss Alps, *Geomorphology*, *132*, 208–221.
- Scott, W. J., P. Sellmann, and J. A. Hunter (1990), Geophysics in the study of permafrost, in *Geotechnical and Environmental Geophysics*, vol. 1, *Review and Tutorial, Invest. Geophys.* 5, pp. 355–338, Soc. of Explor. Geophys., Tulsa, Okla.
- Sevruck, B. (1986), Correction of precipitation measurements: Summary report, Zürcher Geographische Schriften, report 23, pp. 13–23, ETH, Zurich, Switzerland.
- Sheehan, J. R., W. E. Doll, and W. A. Mandell (2005), An evaluation of methods and available software for seismic refraction tomography, *J. Environ. Eng. Geophys.*, *10*(1), 21–34.
- Simmons, C. S., and P. D. Meyer (2000), A simplified model for the transient water budget of a shallow unsaturated zone, *Water Resour. Res.*, *36*, 2835–2844.
- Sloan, P. G., and I. D. Moore (1984), Modeling subsurface stormflow on steeply sloping forested watersheds, *Water Resour. Res.*, *20*, 1815–1822, doi:10.1029/WR020i012p01815.
- Sueker, J. K., J. N. Ryan, C. Kendall, and R. D. Jarrett (2000), Determination of hydrological pathways during snowmelt for alpine/subalpine basins, Rocky Mountain National Park, Colorado, *Water Resour. Res.*, *36*, 63–75.
- Symes, W. W. (2008), Migration velocity analysis and waveform inversion, *Geophys. Prospect.*, *56*(6), 765–790, doi:10.1111/j.1365-2478.2008.00698.x.
- Tanarro, L. M., M. Hoelzle, A. García, M. Ramos, S. Gruber, A. Gomez, M. Piquer, and D. Palacios (2001), Permafrost distribution modelling in the mountains of the Mediterranean Corral del Veleta, Sierra Nevada, Spain, *Norw. J. Geogr.*, *55*, 253–260, doi:10.1080/00291950152746612.
- Tarboton, D. G. (1997), A new method for the determination of flow directions and upslope areas in grid digital elevation models, *Water Resour. Res.*, *33*, 309–319, doi:10.1029/96WR03137.

- Tonidandel, D., J. Leitner, V. Mair, and K. Lang (2010), Erste Ergebnisse der Kernbohrung auf dem aktiven Blockgletscher in Lazaun, Schnalstal (Südtirol) [First results of borehole stratigraphies at an active rock glacier in Lazaun, Schnals valley (South Tyrol)], *GeoAlp*, *7*, 106–107.
- Vonder Mühl, D., C. Hauck, and H. Gubler (2002), Mapping of mountain permafrost using geophysical methods, *Prog. Phys. Geogr.*, *26*, 643–660, doi:10.1191/0309133302pp356ra.
- Walvoord, M. A., and R. G. Striegl (2007), Increased groundwater to stream discharge from permafrost thawing in the Yukon River basin: Potential impacts on lateral export of carbon and nitrogen, *Geophys. Res. Lett.*, *34*, L12402, doi:10.1029/2007GL030216.
- Watkins, J. S., L. A. Walters, and R. H. Godson (1972), Dependency of in-situ compressional-wave velocity on porosity in unsaturated rocks, *Geophysics*, *37*(1), 29–35.
- Western, A. W., R. B. Grayson, and T. R. Green (1999), The Tarrawarra project: High resolution spatial measurement, modelling and analysis of soil moisture and hydrological response, *Hydrol. Processes*, *13*, 633–652, doi:10.1002/(SICI)1099-1085(19990415)13:5<633::AID-HYP770>3.0.CO;2-8.
- Williams, M., M. Knauf, N. Caine, F. Liu, and P. Verplanck (2006), Geochemistry and source waters of rock glacier outflow, Colorado Front Range, *Permafrost Periglacial Processes*, *17*, 13–33, doi:10.1002/ppp.535.
- Yang, D., D. L. Kane, L. D. Hinzman, B. E. Goodison, J. R. Metcalfe, P. Y. T. Louie, G. H. Levesley, D. G. Emerson, and C. L. Hanson (2000), An evaluation of the Wyoming gauge system for snowfall measurement, *Water Resour. Res.*, *36*, 2665–2677.
- Yilmaz, O. (1987), *Seismic Data Processing, Invest. Geophys.*, vol. 2, Soc. of Explor. Geophys., Tulsa, Okla.
- Zhang, T., et al. (2005), Spatial and temporal variability in active layer thickness over the Russian Arctic drainage basin, *J. Geophys. Res.*, *110*, D16101, doi:10.1029/2004JD005642.
- Zhang, X., Z. Nan, J. Wu, E. Du, T. Wang, and Y. You (2012), Mountain permafrost distribution modeling using Multivariate Adaptive Regression Spline (MARS) in the Wenquan area over the Qinghai-Tibet Plateau, *Sci. Cold Arid Reg.*, *4*(5), 361–370, doi:10.3724/SP.J.1226.2012.00361.